Decoding spatial locations from primate lateral prefrontal cortex neural activity during virtual navigation

IOP Publishing J. Neural Eng. 20 (2023) 016054 https://doi.org/10.1088/1741-2552/acb5c2

Journal of Neural Engineering

OPEN ACCESS

RECEIVED
26 July 2022

REVISED
9 January 2023

ACCEPTED FOR PUBLICATION
24 January 2023

PUBLISHED
24 February 2023

PAPER

Decoding spatial locations from primate lateral prefrontal cortex neural activity during virtual navigation

Renée Johnston[1,2,*], **Mohamad Abbass**[3,4,5], **Benjamin Corrigan**[4,5], **Roberto Gulli**[6,7], **Julio Martinez-Trujillo**[4,8] and **Adam Sachs**[1,9]

[1] University of Ottawa Brain and Mind Research Institute, Ottawa, ON, Canada
[2] Ottawa Hospital Research Institute, Ottawa, ON, Canada
[3] Department of Clinical Neurological Sciences, London Health Sciences Centre, Western University, London, ON, Canada
[4] Western Institute for Neuroscience, Western University, London, ON, Canada
[5] Department of Physiology and Pharmacology, Schulich School of Medicine and Dentistry, Western University, London, ON, Canada
[6] Zuckerman Mind Brain Behavior Institute, Columbia University, New York, NY, United States of America
[7] Center for Theoretical Neuroscience, Columbia University, New York, NY, United States of America
[8] Department of Physiology, Pharmacology, and Psychiatry, Schulich School of Medicine and Dentistry, Western University, London, ON, Canada
[9] Division of Neurosurgery, Ottawa Hospital Research Institute, Ottawa, ON, Canada
[*] Author to whom any correspondence should be addressed.

E-mail: rejohnston@ohri.ca

Keywords: invasive brain-computer interface, spatial navigation, lateral prefrontal cortex, non-human primates, support vector machine

Abstract

Objective. Decoding the intended trajectories from brain signals using a brain-computer interface system could be used to improve the mobility of patients with disabilities. *Approach*. Neuronal activity associated with spatial locations was examined while macaques performed a navigation task within a virtual environment. *Main results*. Here, we provide proof of principle that multi-unit spiking activity recorded from the lateral prefrontal cortex (LPFC) of non-human primates can be used to predict the location of a subject in a virtual maze during a navigation task. The spatial positions within the maze that require a choice or are associated with relevant task events can be better predicted than the locations where no relevant events occur. Importantly, within a task epoch of a single trial, multiple locations along the maze can be independently identified using a support vector machine model. *Significance*. Considering that the LPFC of macaques and humans share similar properties, our results suggest that this area could be a valuable implant location for an intracortical brain-computer interface system used for spatial navigation in patients with disabilities.

1. Introduction

Invasive brain-computer interface (iBCI) systems have the potential to improve quality of life for physically disabled individuals. The real-time use of intracortical activity can add communication channels (Santhanam *et al* 2006, Pandarinath *et al* 2017) or control assistive devices (Flint *et al* 2012, Ajiboye *et al* 2017). One potential application of a brain-computer interface (BCI) is to aid individuals with limited mobility to navigate environments. As reported by Al-qaysi *et al* (2018), the current advancement in technology allows intelligent wheelchairs to be safely controlled by brain signals, making it one of the important applications of BCI-based systems that can help disabled individuals gain independence. One issue that remains poorly investigated is the brain areas that can provide reliable signals for spatial navigation via a BCI.

The prefrontal cortex is known to coordinate cognitive processes such as working memory (Miller *et al* 2018) and learning abstract rules (Wallis *et al* 2001, Buschman *et al* 2012). Studies have shown the impact of prefrontal cortex lesions on the successful execution of spatial working memory functions (Curtis and D'Esposito 2003) and that the firing rate of the lateral prefrontal cortex (LPFC) cells is modulated by spatial working memory task demands (Jung *et al* 1998, Corrigan *et al* 2021). More specifically, neurons in the LPFC

have been found to encode remembered spatial locations during working-memory (Mendoza-Halliday and Martinez-Trujillo 2017, Leavitt *et al* 2017b) and visuospatial attention (Tremblay *et al* 2015, Backen *et al* 2018) tasks, as well as movement intentions (Markowitz *et al* 2011, Boulay *et al* 2015, Johnston *et al* 2021). Within the LPFC, neurons encode the location of items in virtual environments (Roussy *et al* 2021) when monkeys navigate toward visible or invisible targets using a joystick. The use of such desktop systems provides an efficient platform to analyze the neuronal activity underlying path-integration (excluding proprioceptive information) during spatial navigation tasks (May and Klatzky 2000, Gulli *et al* 2020). The geometry and intersections of a maze virtual environment, including boundaries (Lee 2017) and landmarks (Jansen-Osmann 2002), are key elements of spatial mapping and navigation behavior. Historically, motor execution tasks allowed the research community to create primary and supplementary motor cortex functional maps. Further research demonstrated that motor imagery and motor attempt can generate valuable brain activity for the discrimination of movement intention (Chen *et al* 2021), particularly applicable to BCI systems. We can use a similar approach for spatial navigation, by starting with the question of how spatial locations can be decoded while navigating a virtual maze using a joystick. The results can then guide us to further test imagined or attempted navigation.

Here, we demonstrate that spatial locations and task relevant events can be decoded from multichannel LPFC activity of rhesus macaques navigating through a virtual environment using a joystick. Using support vector machine (SVM) learning, we found that spatial location identification is more precise for locations associated with task relevant information such as maze intersections and directional change. We also demonstrated that different maze locations for the same task event could be differentiated (i.e. two different starting locations). Since spatial location probability depends on the prior position, we added a Markov chain to the SVM model prediction and found that it improves the decoder performance. We also show the possibility to optimize the size of the feature set by projecting the multi-unit spiking rate on canonical vectors generated to maximize the difference between spatial locations on the maze. The outcome of this study highlights the possibility of using the prefrontal cortex as a source of information related to task-relevant locations in a goal-selective cognitive iBCI system.

2. Methods

2.1. Animals

Two male rhesus macaques (*Macaca mulatta*), aged 10 and 9 years old with respective weights of 12 kg and 10 kg, were trained to navigate through a maze with a joystick to complete an associative memory task (figure 1(a)). For this task, the primates were trained to associate a context with a disk color. The goal was to reach the correct colored disk depending on the wall texture observed in the corridor of the maze (figure 1(b)). If successful, the monkeys would receive a juice reward.

2.2. Electrophysiological recordings

The brain activity from the LPFC was recorded using two Utah microelectrode arrays (96 channels, electrode length of 1.5 mm). They were both implanted anterior to the arcuate sulcus, the first microelectrode array (MEA0) and second (MEA1) being placed lateral and medial to the principal sulcus respectively (figure 1(c)). The neuronal signals were recorded using a 128-channel Cerebus Neuronal Signal Processor from Blackrock Microsystems. The Plexon offline sorter was used to isolate the single units from the multi-unit stream. The local field potential (LFP) signal was band-pass filtered (0.3 Hz to 7.5 kHz) and digitized (16-bit with 1 μV per bit) at 30 kHz. Using a fourth-order Butterworth anti-aliasing filter with a 250 Hz cut-off frequency, the signal was finally down sampled to 1 kHz and re-reference to the common average.

2.3. Experimental setup

The behavioral task took place in an *X* maze virtual environment (Doucet *et al* 2016). During a session, the rhesus macaques were seated in a custom-built chair facing a computer monitor, the animals' head being fixed to allow eye position recordings which were not used in our study. They would freely navigate the maze using a two-axis joystick. The position within the maze was recorded at a rate of 75 Hz, matching the monitor refresh rate.

2.4. Behavioral task

The task required associating a context (wall texture options: wood or steel) with a correct destination (disk options: color1 or color2). A session would include multiple blocks (3 or 4), each block had a different set of association (context-color) to be learned. Note that the first and last blocks would use the same association set. The animals would receive a juice reward only if the correct association was made.

A trial starts once the monkey has completed the previous trial (figure 1(d)), rotating its point of view to face the center of the maze ('post reward' task epoch). The animal then navigates from the left or right branch at one end of the *X* maze to the branch junction ('start of trial' task epoch). The monkey continues through a long corridor in which the side walls' texture represents the trial context ('context showing' task epoch). At the end of the corridor, the colored disks are visible ('goal showing' task epoch). The monkey then travels through the left

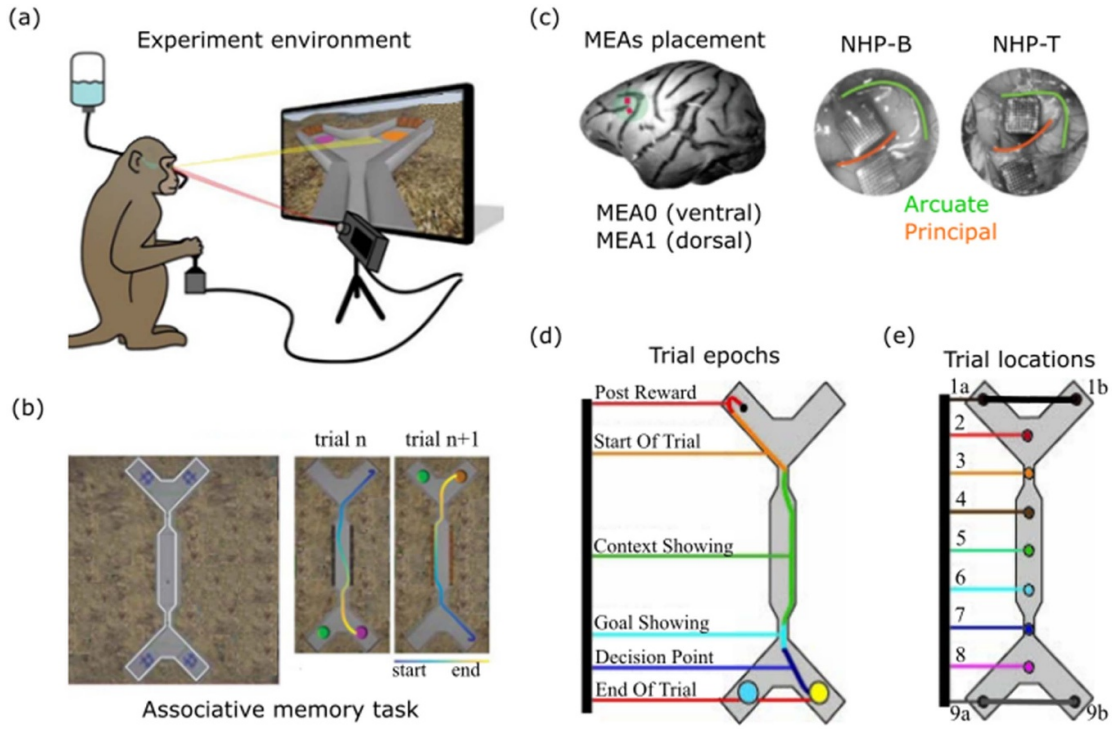

Figure 1. Experiment description and intracortical implant locations details. (a) Virtual desktop environment allowed the monkey to navigate through the maze using a joystick. Eye movements were tracked (Gulli *et al* 2020). (b) One trial of the associative memory task would start at one end of the maze and move to the other end of the maze while the monkey learned to associate the correct wall context texture in the corridor of the maze with the correct disk color to obtain a reward. The next trial would start when the animal reached the disk and start its rotation back to face the maze center (Gulli *et al* 2020). (c) MEAs were chronically implanted anterior to the arcuate sulcus in the LPFC of NHP-B and NHP-T, MEA0 and MEA1 located lateral and medial to the principal sulcus (Roussy *et al* 2021). (d) Schematic of the maze showing trial epochs. (e) Schematic of the maze showing trial locations considered.

or right end branch, depending on learned context-color association ('end of trial' task epoch). The next trial starts once the monkey reaches a colored disk. The context and the disk-color branch location were randomized independently for each trial. Equally spaced maze locations along the North–South axis were selected (figure 1(e)).

Neural activity associated with task events and spatial locations is independent of the successful completion of the task. For this reason, we considered all trials regardless of the successful association of the context with a color. We only excluded incomplete trials where the animals did not navigate through all task locations. There was no time limit for a trial, the macaques would typically traverse the maze at the same speed, from the start to the end of each trial. The incomplete trials would be caused by the experimenter interrupting the experiment (i.e. when sufficient trials had been captured). Learning and unlearning activity was present during the trials but not considered in the analysis of spatial locations along the maze and the epochs of the task.

A session included the same navigational requirement but from trials belonging to different color-context associative tasks. We processed one session for each monkey. For non-human primate Buzz (NHP-B), the session included three blocks run in the following order: block1 (66 trials), block2 (288 trials), and block3 (68 trials). For non-human primate Theo (NHP-T), the session included four blocks sequentially presented as follow: block1 (40 trials), block2 (97 trials), block3 (319 trials), and block4 (61 trials). Note that block1 and block3 for NHP-B, as well as block1 and block4 for NHP-T, used the same color-context association.

2.5. Neural data analysis

MATLAB and RStudio were used for all data analysis.

2.5.1. First principal spectral component

As reported by Miller *et al* (2014), this signal represents the overall broadband frequency activity for a window centered at a particular time. For each 1024 ms window of interest, a principal component analysis was performed on the normalized power spectrum of the LFP to obtain the eigenvectors and eigenvalues. The first principal spectral component refers to the original spectrum projected on the principal eigenvector. For a more detailed description refer to Miller *et al* (2009).

2.5.2. SVM classification

To identify the spatial locations and epochs from the single and multi-unit spiking rate or from the first principal spectral component of the LFP, we used a SVM algorithm with a linear kernel (LIBLINEAR

implementation for MATLAB (Fan *et al* 2008), with options L2-regularized, L2-loss, and five-fold cross-validation). We chose this algorithm as it is fast and is less vulnerable to overfitting. To classify multiple classes, this algorithm uses the one-vs-rest strategy.

2.5.3. Markov chain

The probability to be at a specific location in a maze depends on the prior location. For that reason, we added a stochastic model to our decoder. We designed a simple Markov chain which assigned probabilities for all possible locations given a prior location. Our predicted location is then based on the multiplication of the Markov chain probabilities with the SVM prediction probabilities.

2.5.4. Canonical discriminant analysis

To reduce the size of the SVM feature set used to decode the spatial locations, we generated eight canonical vectors for each microelectrode array that maximize the neuronal activity difference between the nine locations. In RStudio, we first fitted a linear model using the function '*lm*' from the R Stats package (Wilkinson and Rogers 1973, Chambers 1992) and then performed a canonical discriminant analysis (Ramsay and Silverman 1997) using the '*candisc*' function from the R candisc package (Friendly and Fox 2020) to create the canonical vectors. See Johnston *et al* (2021) for further implementation details.

2.6. Statistics

The statistical significance of SVM feature set distributions was evaluated using the MATLAB implementation of the Wilcoxon rank sum test (Wilcoxon 1945). Each entry in our distributions was the average decoding accuracy of the five-fold SVM result, which was repeated 100 times to create a full distribution for this feature set. A null distribution was similarly calculated using the average accuracy of the five-fold SVM results after shuffling the classifier labels. Before performing the Wilcoxon rank sum test between our feature sets, the average of the null distribution was subtracted from the decoding accuracy distribution. The statistically significant threshold was reported when the resulting p-value from the Wilcoxon test was less than 0.01.

3. Results

3.1. Spatial locations within a virtual environment can be decoded from the LPFC neural activity

To explore whether a subject's position can be decoded from neuronal activity in the LPFC we trained two macaque monkeys to perform a navigation task in a virtual environment and recorded the responses of neurons in the LPFC using chronically implanted microelectrode arrays. A virtual maze (X-maze) was originally created using a gaming engine (Gulli *et al* 2020, Corrigan *et al* 2021). A trial n consists of a rhesus macaque navigating through the maze using a joystick going from one of two branches on one side at the start of the trial (SOT), to one of two possible branches on the opposite side at the end of the trial (EOT) (figure 1(a)). The maze had a corridor that connected the two sets of branches. The animal had to learn the association between the wall texture (wood or steel) presented when entering the corridor (context epoch) and the colors of two disks that appear when the animals reached the branching point (e.g. wood context means choose the red disk and steel context means choose the green disk). At the end of the trial, the monkey receives a juice reward if the correct colored disk was reached. The next trial ($n + 1$) would start once the monkey had turned around in the maze (figure 1(b)).

The brain activity of each monkey was recorded from two 10 × 10 microelectrode arrays (Maynard *et al* 1997, Normann *et al* 1999) located in the LPFC anterior to the knee of the arcuate sulcus. MEA0 and MEA1 are the array designations lateral and medial to the principal sulcus respectively (figure 1(c)). For the session with NHP-B, the electrophysiological recording from the first array (MEA0) provided valid signals from 96 electrodes (97 single-units, 96 multi-units), while the second array (MEA1) gave 95 channels (132 single-units and 95 multi-units). For the session with NHP-T, the electrophysiological recording from MEA0 provided valid signals from 91 electrodes (90 single-units and 91 multi-units), while MEA1 gave 96 channels (49 single-units and 96 multi-units).

For each trial, 5 task epochs (figure 1(d)) and 11 maze positions (figure 1(e)) were defined on the North–South axis from where the animal started his navigation to where the animal stopped moving forward at the end of the trial. Note that the trials for location 1 and 9 are split between the right branch (locations 1a/9a) or left branch (locations 1b/9b) depending on the specific trial (figure 2(a)).

We first examined if spatial locations within the maze could be decoded from the brain signals. We looked at single unit spiking activity around each maze location (1024 ms window) and found some single units which had higher number of spikes around specific locations. Figures 2(b) and (c) show examples of a single unit tuned to location 8 and location 9b respectively.

We then used five-fold cross-validation SVM repeated 100 times to evaluate the average decoding accuracy of 11 spatial locations from features based on a 1024 ms window of single-units and multi-units spiking rates as well as the first principal spectral component of the LFP (Miller *et al* 2009) at those places. In a real-time BCI application, avoiding spike sorting is beneficial because it is time consuming. We therefore compared the average decoding accuracy obtained with the different features on individual blocks for both animals (figure 2(h)). The tested

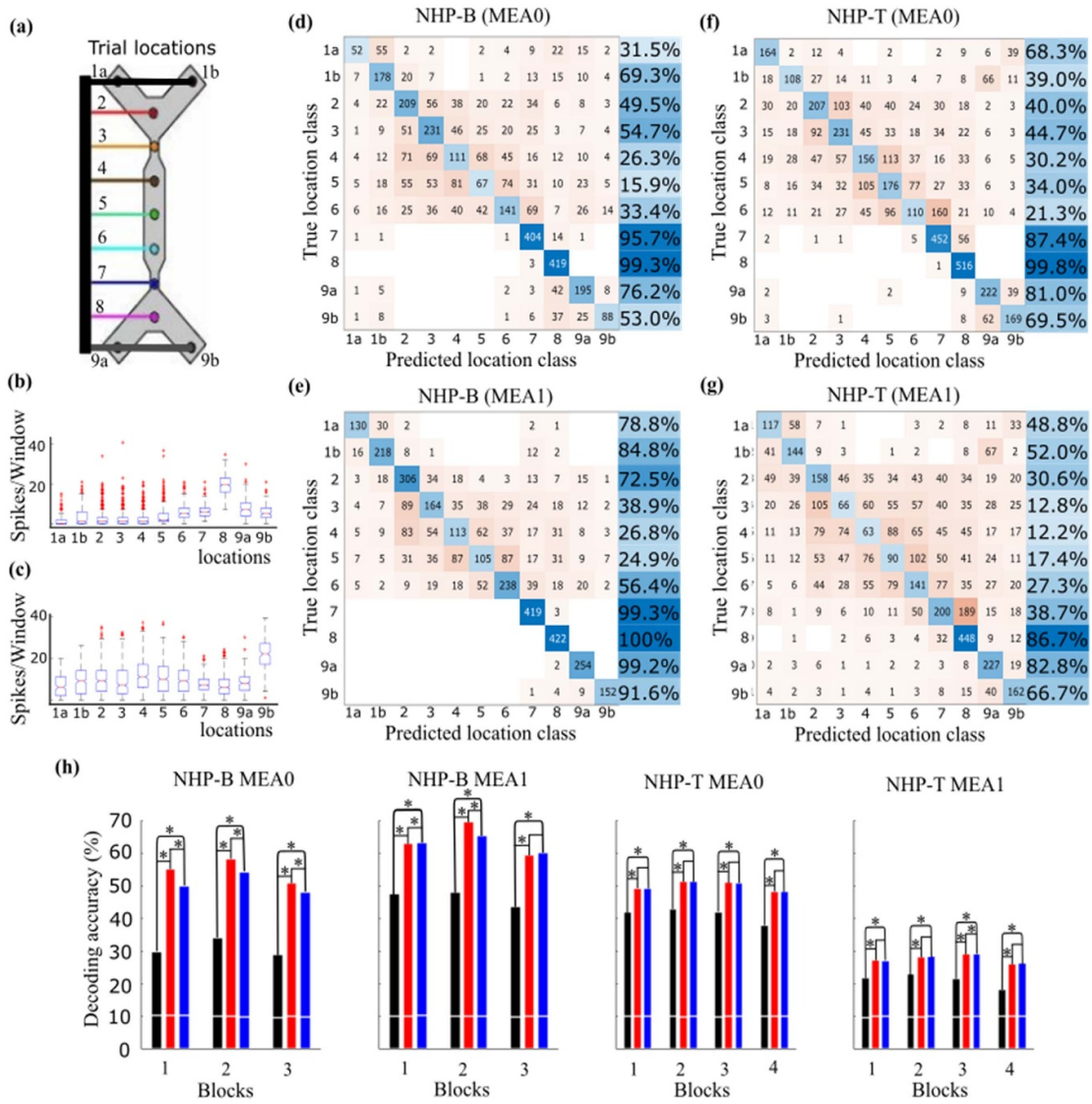

Figure 2. SVM decoding of locations from PFC neuronal activity. (a) Schematic of the maze showing the location points considered in our decoding. (b), (c) Single unit examples showing the number of spikes per 1024 ms window statistical distribution centered at each location (NHP-B, 422 trials). (d), (e) Confusion matrices showing true and predicted classes of decoding the locations using multi-unit spiking activity from 422 trials (all blocks) with NHP-B MEA0 and MEA1 respectively. The diagonal values represent the number of trials where the prediction was successful (darker blue shows higher percentage of successful trials for each class). (f), (g) Confusion matrices showing location decoding from 517 trials (all blocks) with NHP-T MEA0 and MEA1 respectively. (h) Overall decoding accuracy of locations obtained using the first principal spectral component of the LFP signal (black), single-unit (red) and multi-unit (blue) spiking activity from a 1024 ms window. White horizontal lines show the respective shuffled result ($p < 0.001$ is represented by *).

feature sets on individual blocks for both arrays were all significantly higher than predicted by chance, however, the LFP-based decoder performed worse than that of the spiking activity. For most blocks, single units provided better results than multi-units. Nevertheless, the remaining analysis and presented results will focus on multi-unit activity because of the broader applicability for a future iBCI.

The confusion matrices in figure 2 show the results of the predicted versus true decoded classes of each location using data from all blocks for NHP-B on MEA0 (figure 2(d)), MEA1 (figure 2(e)), and for NHP-T on MEA0 (figure 2(f)) and MEA1 (figure 2(g)). The results highlight the fact that some locations are associated with unique neural activity, while others are associated with activity that resembles other locations. Similarity of activity is often seen in the long corridor of the maze (locations 4–6). Locations associated with the start of trial up to entering the corridor (locations 1–3) and from the goal showing to end of trial (locations 7–9) are better decoded. Importantly, the initial starting branch during the SOT epoch (locations 1a/1b) and the ending branch during EOT epoch (locations 9a/9b) could be particularly well identified on NHP-B MEA1 (start right: 78.8%, start left: 84.8%, end right: 99.2%, end left: 91.6%). These findings eliminate the possibility that the locations were decoded from neuronal activity linked with the time to reward or linked with the task epoch of the trials.

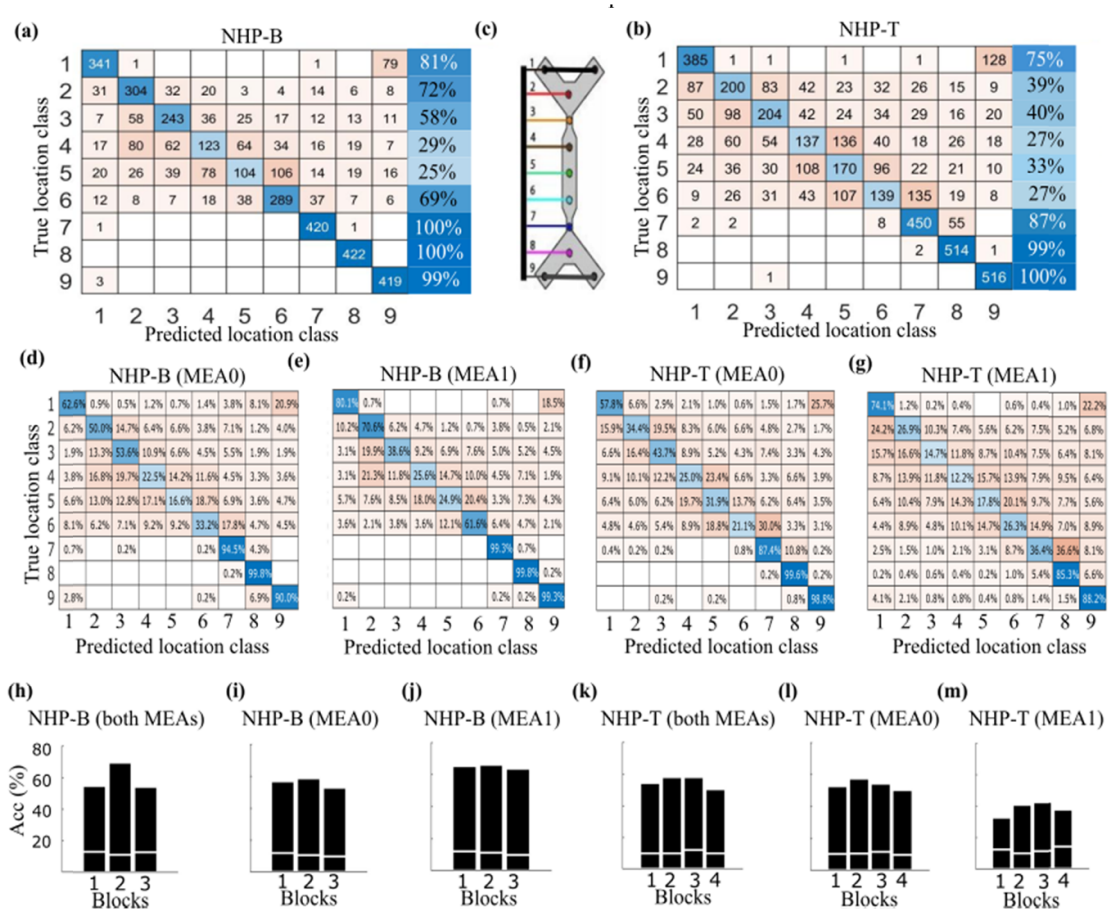

Figure 3. SVM decoding of locations from individual and combined blocks, using single or both arrays. (a) Confusion matrix showing true and predicted classes of decoding the 9 locations from 422 trials (all blocks) using both arrays on NHP-B. Right blue column show decoded accuracy for each class. Overall decoding accuracy obtained was 70%. (b) Confusion matrix showing true and predicted classes of decoding the 9 locations from 517 trials (all blocks) using both arrays on NHP-T. Right blue column show decoded accuracy for each class. Overall decoding accuracy obtained was 59%. (c) Schematic of the maze showing the location points considered for this analysis. (d), (e) Confusion matrices showing predicted and true location decoding accuracy from 422 trials (all blocks) on NHP-B MEA0 and MEA1 respectively. (f), (g) Confusion matrices showing predicted and true location decoding accuracy from 517 trials (all blocks) on NHP-T MEA0 and MEA1 respectively. (h) SVM decoding accuracy for individual blocks using both arrays for NHP-B. The horizontal white lines show the accuracy when labels were shuffled. (i), (j) SVM decoding for individual blocks on NHP-B MEA0 and MEA1 respectively. (k) SVM decoding accuracy for individual blocks using both arrays for NHP-T. (l), (m) SVM decoding for individual blocks on NHP-T MEA0 and MEA1 respectively.

For subsequent analyses, we balanced the dataset by comparing the activity at 9 locations (instead of 11) on the North–South axis, combining the initial and final left/right branches into single locations (figure 3(c)). The results of this analysis reinforced that location can be decoded well from the neural activity. Using the data from all blocks and both arrays, the decoding accuracies for positions 1, 7, 8, 9 (the starting point and the end of the corridor to the final point of the trial), are all above 81% for NHP-B (the last three locations being decoded accurately for 964 out of 966 trials) and above 75% for NHP-T (figures 3(a) and (b)). To highlight the impact of array placement on the decoding accuracy results, we looked at the predicted and true location class from all blocks on primates NHP-B (MEA0: figure 3(d), MEA1: figure 3(e)) and NHP-T (MEA0: figure 3(f), MEA1: figure 3(g)). Different levels of decoding accuracy were obtained with individual arrays, but all arrays could best discriminate locations 1-7-8-9. The decoding accuracies of locations from the combined blocks and arrays (figures 3(a) and (b)) are mainly the combination of the best decoding accuracies obtained from individual arrays.

We calculated the overall decoding accuracy by (a) performing a five-fold cross-validation SVM analysis, (b) averaging the returned five-fold accuracies and then (c) repeating this process 100 times to obtain a distribution of results, reporting its mean as the accuracy. The standard deviations of the obtained accuracy distributions for all blocks were smaller than 1.5%. The overall decoding accuracy using data from individual and combined arrays are significantly above the shuffled results for all individual blocks (figures 3(h)–(m)). We evaluated the above chance accuracy distributions by subtracting each entry with the averaged shuffled accuracy. The Wilcoxon rank sum showed that the difference between the above

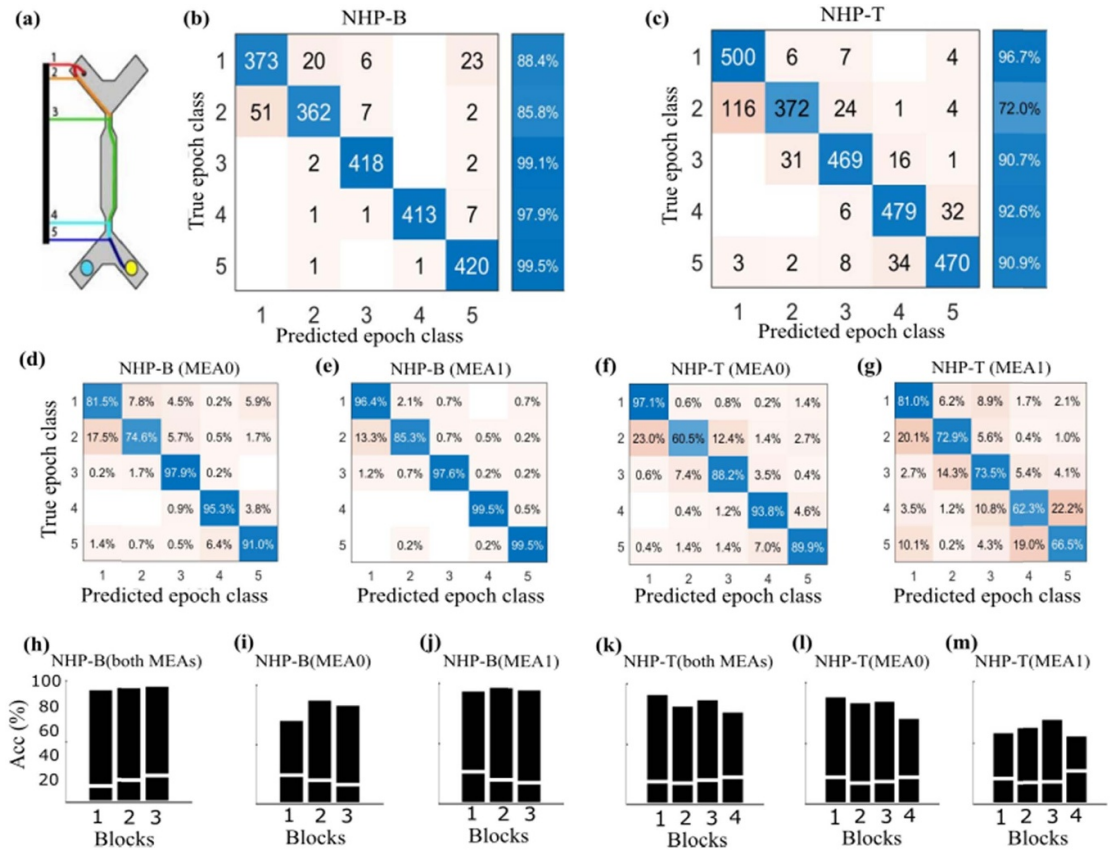

Figure 4. SVM decoding of epochs from individual and combined blocks, using single or both arrays. (a) Schematic of the maze showing the task epochs onset considered for this analysis. (b) Confusion matrix showing true and predicted classes of decoding the epochs from 422 trials (all blocks) using both arrays on NHP-B. Overall decoding accuracy obtained was 94.1%. (c) Confusion matrix showing true and predicted classes of decoding the 5 task events from 517 trials (all blocks) using both arrays on NHP-T. Overall decoding accuracy obtained was 88.6%. (d), (e) Confusion matrices showing decoding of the task events for combined blocks on NHP-B MEA0 and NHP-B MEA1 respectively. (f), (g) Confusion matrices showing decoding of the task events for combined blocks on NHP-T MEA0 and NHP-T MEA1 respectively. (h) SVM decoding accuracy (black) and chance (horizontal white lines) for individual blocks using both arrays for NHP-B. (i), (j) SVM decoding for individual blocks on NHP-B MEA0 and MEA1 respectively. (k) SVM decoding accuracy for individual blocks using both arrays for NHP-T. (l), (m) SVM decoding for individual blocks on NHP-T MEA0 and MEA1 respectively.

chance accuracy distributions from individual array compared to using both arrays were all statistically significant ($p < 0.01$).

When analyzing individual arrays, we found that data captured from MEA1 of NHP-B and MEA0 of NHP-T produced a slightly better overall performance compared to their counterparts in the same monkey (figures 3(j)–(l)). This contrast between primates can possibly be caused by the decoding activity being differently located within the LPFC for individual animals, or by higher levels of noise for different implants. These findings indicate that the spatial information can be decoded from LPFC neural activity.

3.2. Parallel identification of task epochs and maze locations

Since the identification of the locations is particularly strong in areas of the maze associated with important events linked to the successful completion of the task, we decided to analyze the epoch neuronal activity at relevant task events (figure 4(a)). Following the same process described for maze location decoding analysis, we confirmed that the distributions of epoch decoding accuracy compared to its chance level were significantly different for individual and combined arrays ($p < 0.01$). The standard deviations of the obtained accuracy for all blocks were smaller than 3.0%.

The five-fold cross-validation SVM lead to decoding performances of the five epoch transitions at accuracy higher than 94% for NHP-B (figure 4(b)) and 88% for NHP-T (figure 4(c)) when combining all blocks and data from both arrays. To highlight the impact of array placement on the decoding accuracy results, we also looked at the predicted and true epoch class from all blocks on primates NHP-B (MEA0: figure 4(d), MEA1: figure 4(e)) and NHP-T (MEA0: figure 4(f), MEA1: figure 4(g)). We found that all task epochs could be well discriminated except for the SOT which would often be confused (23% for array MEA0 on NHP-T) with the previous task epoch (post-reward). Although the difference between above chance distributions were statistically

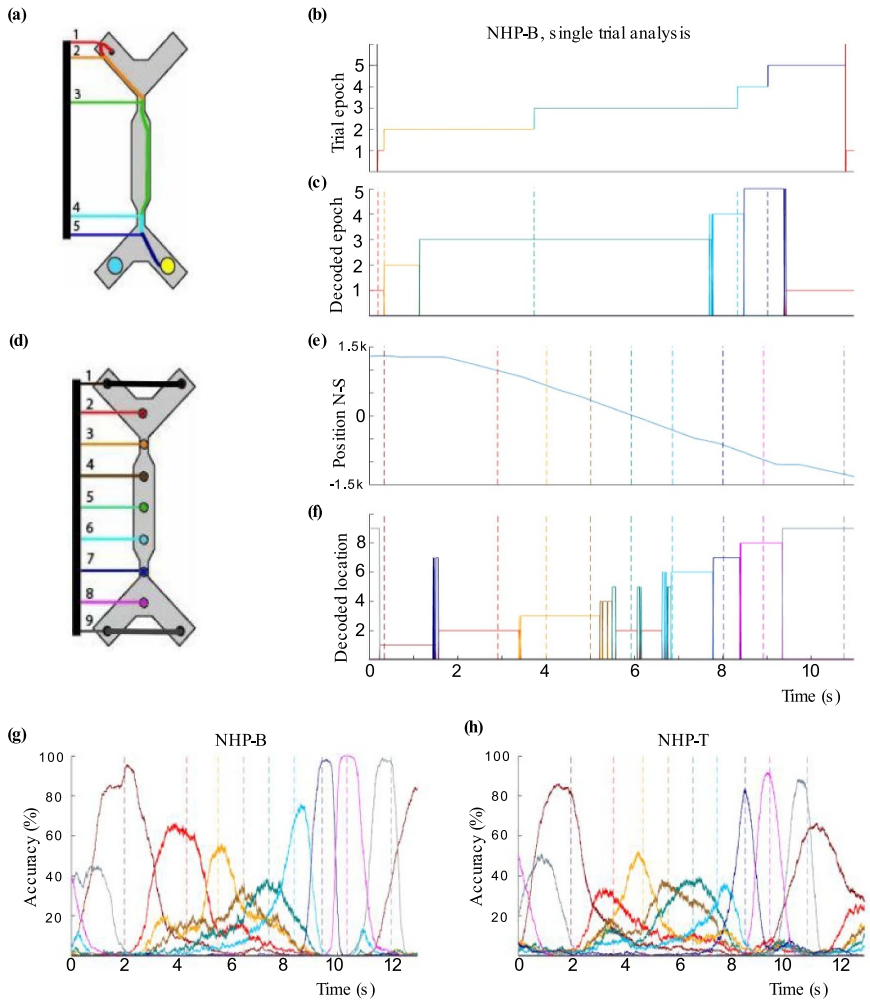

Figure 5. SVM decoding of locations and task epochs over time. Features used in the prediction are spiking rate (1024 ms window) from all available multi-units captured from both MEAs. (a) Schematic of the considered epoch on the maze. (b) Color-coded task epochs over time for an exemplar trial (trial7 of block1 on NHP-B). (c) Prediction of epoch over time for same trial using trained SVM model. (d) Schematic of the considered location points on the maze. (e) Color-coded task locations on the North–South axis of the maze for the same examined trial. (f) Prediction of the maze location over time using trained SVM model. Mean of the decoding accuracy of each location over time, all trials (except training set) being aligned depending on each location for (g) NHP-B and (h) NHP-T.

different, testing individual blocks with combined data from both arrays showed a similar performance between blocks on both animals (figures 4(h)–(k)). However, we found some differences between arrays (NHP-B: figures 4(i) and (j) and NHP-T: figures 4(l) and (m)) which were in line with the results found in our spatial response analysis, possibly caused by higher level of noise on those implants.

To better understand the relationship between activity associated with task events and activity associated with spatial locations, we performed a single-trial decoding analysis. To do this, we used a subset of 200 trials from the block with the largest trial set (block2 and block3 for NHP-B and NHP-T respectively) to train two SVM models to decode the task events and the spatial locations using multi-unit activity from both MEAs. Figure 5(b) shows a typical trial from block1 of NHP-B with its associated task epochs shown on the maze (figure 5(a)). The saved SVM model was used to predict the task epoch for every 10 ms time point of the trial (figure 5(c)). The vertical dashed lines represent the onset of the color-coded task epoch. For this exemplar trial, all onsets of the task events were successfully predicted with the model. Unsurprisingly, in the examined trial, the decision point (epoch #5) quickly becomes decoded as the post reward (epoch #1) for the following trial.

We repeated this analysis for spatial locations. Figures 5(d) and (e) show the maze position over time on the North–South axis of the same exemplar trial. Each vertical dashed line represents one of nine color-coded locations equally spaced on the maze axis and is associated with a particular location point on the maze (figure 5(e)). The classification result (figure 5(f)), evaluated every 10 ms, shows some misclassifications for locations 4–5 but accurate decoding of the other locations. This analysis demonstrates that within a specific epoch of a

trial, it is still possible to decode multiple different locations.

Using the model saved from the prior analysis, we evaluated both primates' average population performance. We tested all trials (excluding the 200 trials used to train the model) and compiled the decoding accuracy around each location point individually. The results highlight the strong decoding at locations that are task-relevant with lower performance while navigating through the long corridor (figure 5(g) for NHP-B and figure 5(h) for NHP-T). The alignment of all trials is based on the position belonging to the exemplar trial. Note that neuronal activity at the first position also caused an increase in predicting the last position associated with the previous trial prior to the maze direction change at the end of the branch. Similarly, the last position of exemplar trial becomes the first position of the next trial, which explains the gradual increase in predicting the first location at the last position.

3.3. Decoding performance improvement with a Markov chain

Since navigation in this task is continuous, the sequence of locations reached at any given time interval is dependent on the probability of moving from one location to the other. If spatial locations were used to control an effector in a BCI system, there would need to be a high level of prediction confidence. We therefore modified the SVM decoder to take advantage of knowledge of previous locations by modifying it with Markov chain inputs. If the prior position is known, the Markov chain probability of a current location is multiplied by the predicted location probability obtained from a trained SVM model.

In the maze task, the position could either be the same or the next forward position since the goal of the task is to move forward. However, in other potential navigation scenarios, there could be the possibility of backward movement or missing the feedback signal of the prior position. We designed a chain with the highest transition probabilities for moving in the forward direction or staying at the same place, and a low probability of moving backward or to the further locations (figures 6(a)–(d)). We tested our trials with and without applying the Markov chain assuming our prior location was either the same (figure 6(f)), the previous (figure 6(e)), or a future location (figure 6(g)). Using features based on the multi-unit activity on both arrays, we averaged the previously saved model decoding accuracy for all trials on individual blocks (excluding the training data). The result of applying the Markov chain is an overall and consistent improvement of our decoding performance on both animals regardless of the prior location being same, forward, or backward.

At the trial level, we repeated the previous analysis on the same example trial (figures 6(h) and (i)), with the addition of the described Markov chain to the prediction path (figure 6(j)). The prediction of locations followed a more regular navigation path. Additionally, location #5, which was missed in the previous non-stochastic decoder, was decoded correctly.

3.4. Canonical space projection of the multi-unit spiking activity

To better understand the number of channels required to decode location, we performed a 'greedy channel analysis' (Leavitt *et al* 2017b). To do this, we first found the individual multi-unit signal which provided the highest decoding accuracy. We saved this first signal deemed our best unit. The decoding accuracy was then evaluated for this unit combined with each remaining unit to find and save what we called our second-best unit. We repeated this process for the third unit up to all units, maximizing the decoding accuracy at each step. The mean accuracy and the 95% confidence level obtained for all blocks are presented for NHP-B (figures 7(a) and (b)) and NHP-T (figures 7(c) and (d)). The results suggest that the peak decoding (stars on figures 7(a)–(d)) is reachable with at most 28 and 34 multi-units for NHP-B and NHP-T respectively (vertical dashed lines figures 7(a)–(d)). In all cases, most of the decoding accuracy is achieved with around ten units.

Having shown that each unit provides its own contribution for decoding the locations and that only a subset of the population is required to reach the peak decoding accuracy, we investigated the possibility to improve processing requirement using canonical space vectors. To identify nine locations, the canonical discriminant analysis of each array generates eight vectors of size equal to the number of multi-units. This canonical space analysis produces weights that maximize the unit activity differences for decoding all the considered spatial locations. SVM features based on the spiking rate projected on these vectors are then used to decode the locations more efficiently (factor reduction of 12 for one array: #multi-units/#canonical vectors). Consistent in both animals and arrays, the projection of the multi-unit spiking activity on the top 2 canonical vectors for 100 trials (figures 7(e)–(h)) demonstrates better separation for locations 1, 7, 8, 9 in line with our previous SVM decoding results. The trial grouping for locations on individual array seem to also reflect the stronger decoding performance on MEA1 for NHP-B (figure 7(f)) and on MEA0 for NHP-T (figure 7(g)) mainly by improving the grouping and showing some separation for location 6. Note that the projection on the other vectors would improve the location separation further but the top two vectors provide approximately 79% of the cumulative variance explained (NHP-B MEA0: 79.7%, MEA1: 79.6%, NHP-T MEA0: 79.1%, MEA1: 78.9%).

We compared the SVM accuracy performance for decoding nine locations from features based on

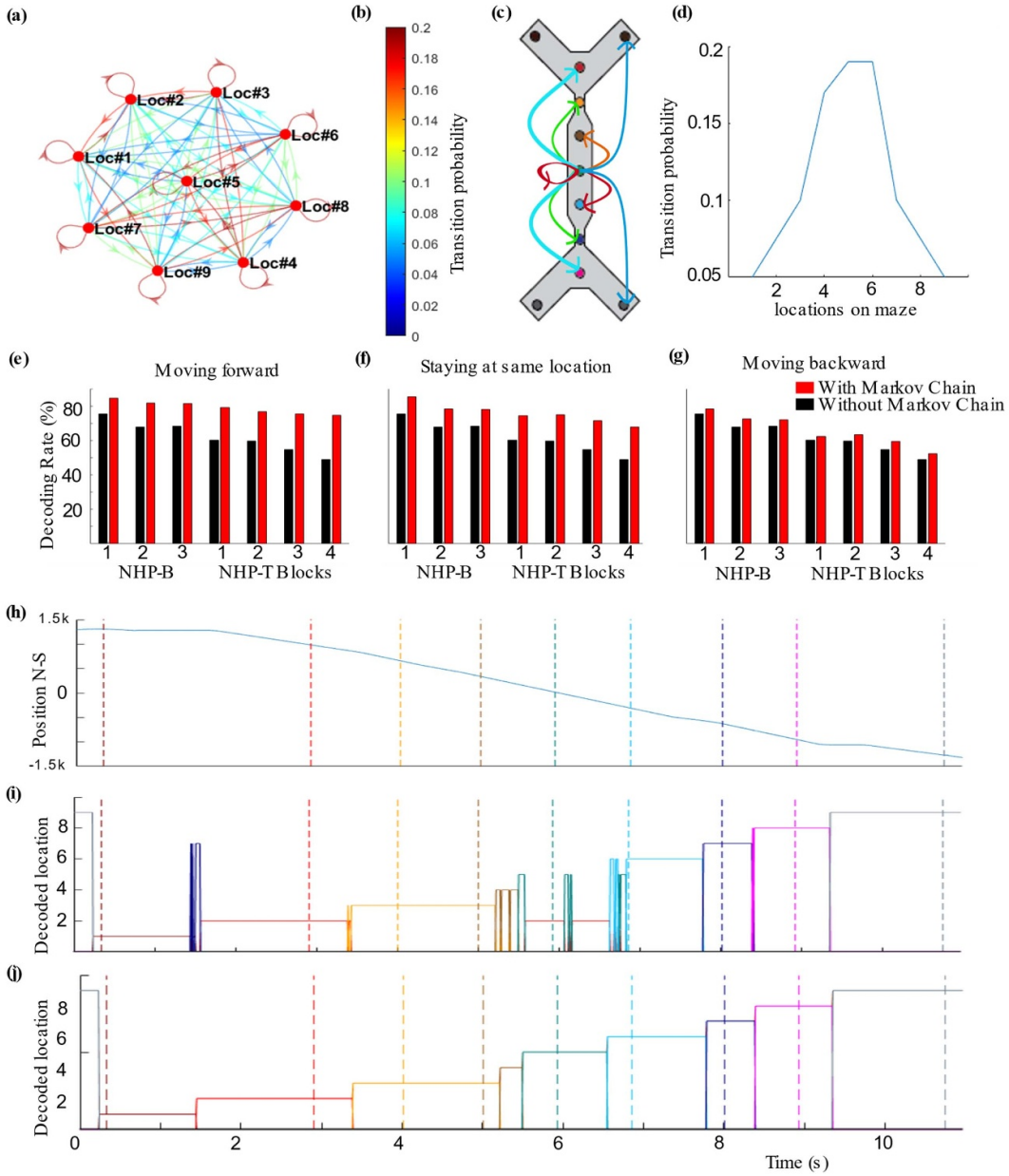

Figure 6. Markov chain impact on spatial locations decoding. (a) Discrete-time Markov chain for the nine locations showing the transition probabilities between nodes. (b) Transition probability color code legend. (c) Schematic of maze showing the transition probabilities if the prior is at location #5. (d) Showing the probability to move from location #5 to any other locations on the maze. Decoding accuracy obtained originally (black) and with the Markov chain added to the prediction (red) for all blocks on both NHPs using multi-unit data from both arrays assuming that (e) the prior was the previous location (moving forward), (f) the prior was the same location (staying still) and (g) the prior was the next location (moving backward). (h) Color-coded task locations on the North–South axis of the maze for the examined trial in previous analysis (figure 5). (i) Prediction of the maze location over time using trained SVM model only. (j) Prediction of the maze location over time adding a Markov chain to SVM prediction.

the multi-unit spiking rate against features from the canonical space projections. For each feature set and its shuffled counterpart, we first performed a five-fold cross-validation SVM analysis and averaged the returned five-fold accuracies. We then repeated this process 100 times to obtain a distribution of results, reporting its mean as the accuracy. The locations were decoded using data from individual blocks on each array. We also applied the decoder to both arrays (figure 8, second column), individual arrays with the blocks combined (figure 8, third column), and combined arrays and blocks (figure 8, fourth column). The statistical analysis distribution of all pairs showed small but statistically significant differences between methods ($p < 0.01$). Overall, the canonical space projections were slightly less reliable, possibly due to the change in the multi-unit contribution between the trials used to train the canonical vectors, and the tested trials. However, this method required a much smaller feature set, which could be advantageous for real-time applications.

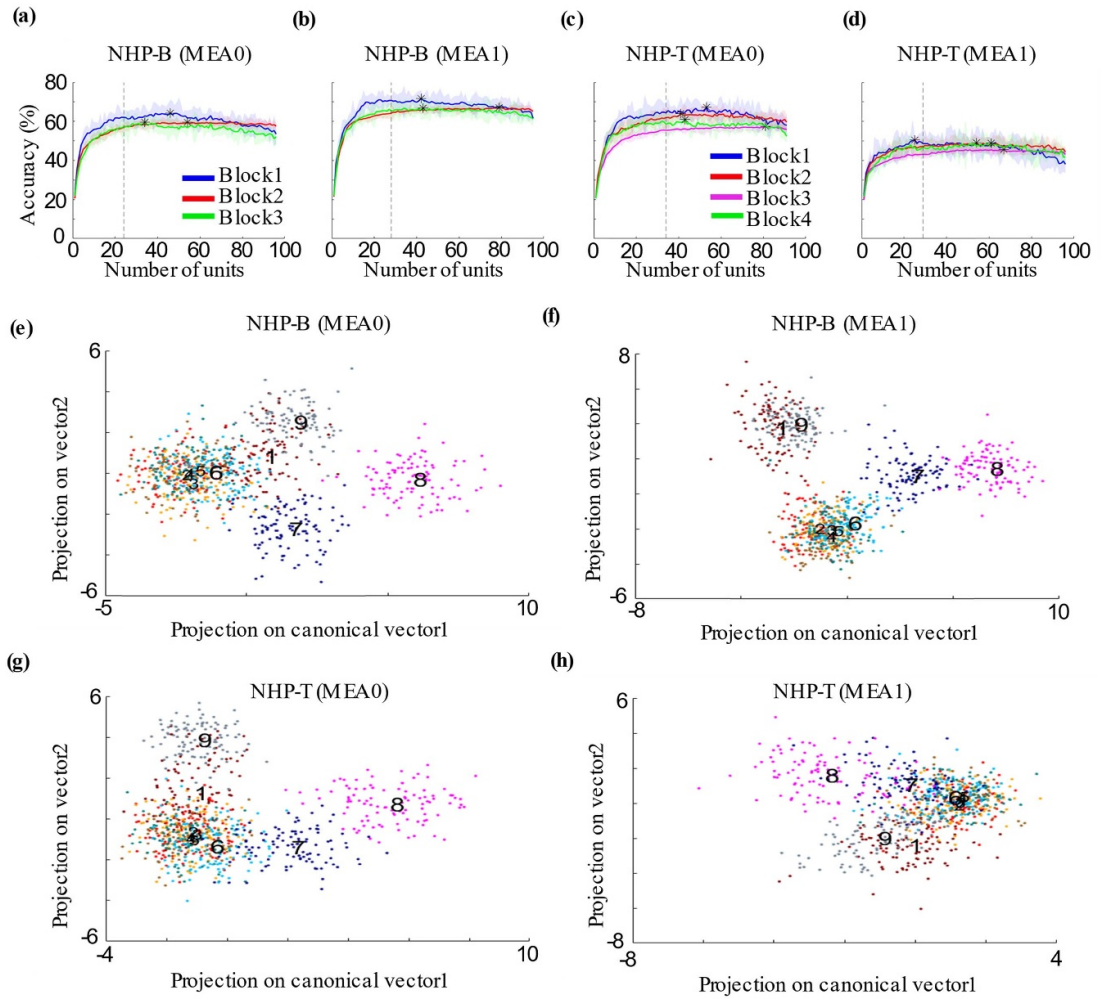

Figure 7. Multi-unit contribution analysis. Decoding accuracy for increasing multi-units for (a) NHP-B (MEA0), (b) NHP-B (MEA1), (c) NHP-T (MEA0), (d) NHP-T (MEA1). Projections in the canonical space of the multi-unit activity for 100 trials at locations 1–9 on monkeys (e) NHP-B (MEA0), (f) NHP-B (MEA1), (g) NHP-T (MEA0), (h) NHP-T (MEA1).

4. Discussion

We examined the neuronal activity in non-human primates' LPFC while they freely navigate through a virtual maze. While the LFP based signal and spiking activity of the population showed selectivity for maze locations, use of the latter provided better decoding accuracy of different spatial positions along the maze. We also demonstrated that decoding of spatial locations from neural activity improves using a Markov chain model. We focus on multi-unit spiking rate as this signal is well suited for the real-time demands of an iBCI system.

4.1. Decoding of space in the primate brain

Previous studies have reported that decoding of spatial positions is possible by reading out the spiking activity of place cells in brain areas such as the hippocampus of rodents during spatial navigation tasks (O'Keefe and Dostrovsky 1971, Buzsáki and Moser 2013, Spellman *et al* 2015). Studies of spatial navigation in primates are scarcer, and the activity of hippocampus cells has been associated with encoding of gaze-position (Ekstrom *et al* 2003, Rolls and Xiang 2006), while other studies have demonstrated encoding of spatial location modulated by the contingencies of the task (Rolls and Wirth 2018, Baraduc *et al* 2019, Gulli *et al* 2020). Although the hippocampus may seem, at first glance, an appropriate target for a BCI that supports spatial navigation, its location, deep in the temporal lobe, makes it less accessible to surgeries and chronic implants with many electrodes.

Other studies have shown that it is possible to build a BCI that utilizes neural activity recorded in premotor areas of macaque monkeys to navigate a cart through a physical environment (Rajangam *et al* 2016). The premotor cortex directly receives information from the LPFC about the conceptual planning of movements to locations (Nakayama *et al* 2008). In principle, it is reasonable to assume the LPFC and the premotor cortex, nearby and posterior to the arcuate (Petrides 2005) work in tandem in the planning and execution of commands for spatial navigation.

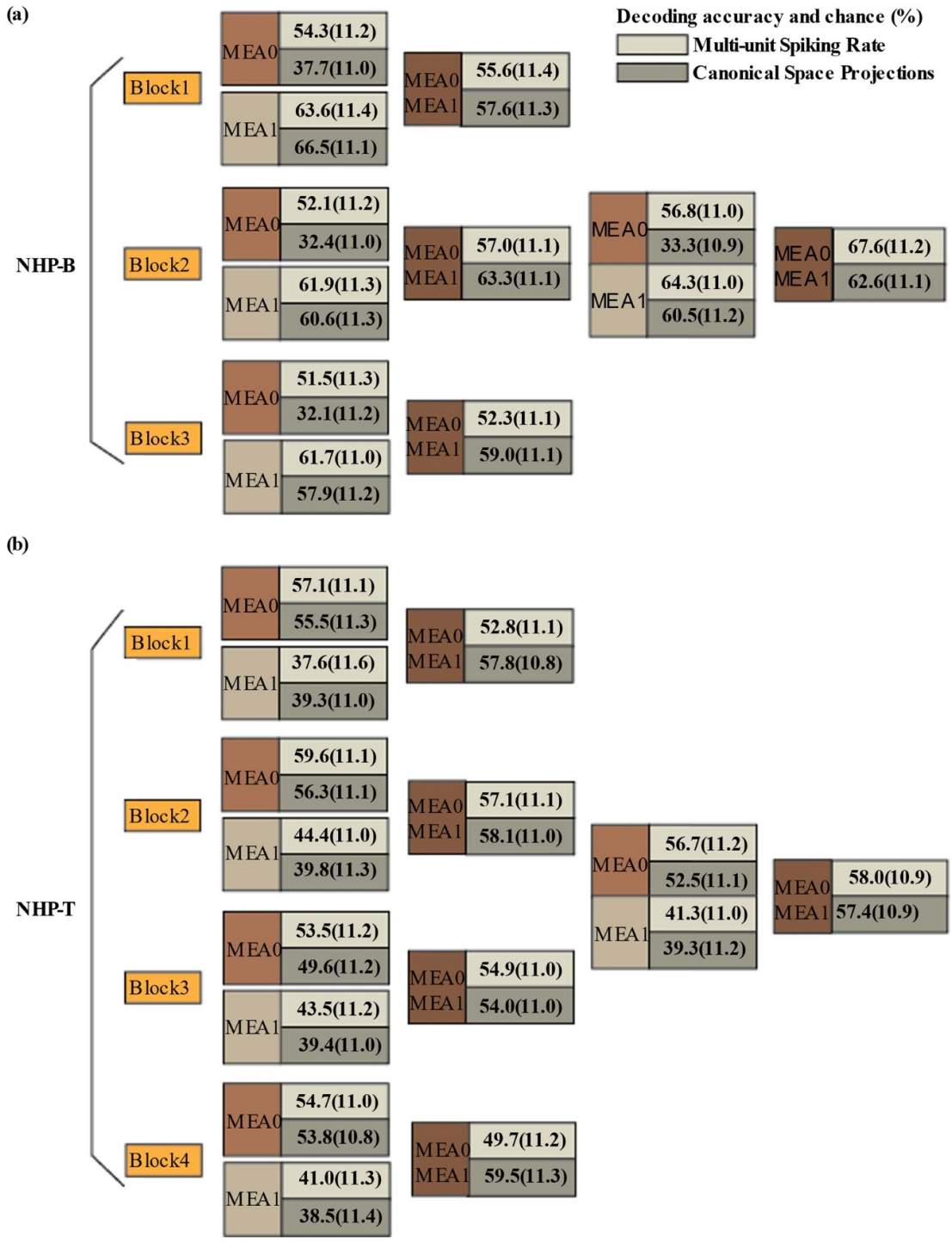

Figure 8. Comparison of SVM decoding using features based on multi-unit spiking rate versus their canonical space projections. Breakdown of decoding accuracy (chance level from shuffling the labels) from individual blocks on individual arrays to data from all blocks on both arrays for (a) NHP-B, and (b) NHP-T. All compared pair distributions were statistically different ($p < 0.001$).

Previous research has shown that task epochs and target locations can be decoded from LPFC activity in macaques (Lennert and Martinez-Trujillo 2013, Boulay *et al* 2015, Johnston *et al* 2021, Roussy *et al* 2021). Recently, Vogel *et al* (2022) demonstrated that neurons in the mouse prefrontal cortex are required for maintenance, encoding, and retrieval of information in spatial working memory. They also reported that in their spatial working memory task, the rodent's spatial position in the physical maze had the largest influence on the prefrontal cortex neuronal activity.

The population decoding of locations during virtual navigation was, to our knowledge, never examined before. We demonstrated that 11 spatial locations along the North–South axis of a virtual maze could be decoded using five-fold cross-validation SVM classifiers. Decoding was higher at

locations where behavior associated with specific task events and reward took place. The prefrontal cortex is known to respond to reward expectation (Leon and Shadlen 1999, Watanabe 2007). The successful decoding of the starting and ending branch (left or right) during the post reward and end of trial epochs of the task eliminate the possibility that this selectivity was associated with the trial time to reward.

The five epochs associated with the key task events could also be identified from the same population. To understand the dependencies of epoch related neuronal activity on locations we looked at the decoding of their parallel identification in a single trial using a saved SVM model. Our results showed that within the same task event, multiple locations can be identified.

Most BCI implementations decode the movement intentions from motor cortex neuronal activity to control assistive devices (Collinger *et al* 2013, Shenoy *et al* 2013). Recently, studies have demonstrated the possibility to better guide iBCI effectors using discrete movement intentions (Fan *et al* 2014), states (Kao *et al* 2017, Sumsky *et al* 2017), transitions (Kang *et al* 2015), and goals (Andersen *et al* 2019) decoded from other cortical areas of the brain. In line with this strategy, our results show that spatial locations within a physical or virtual environment can be deciphered from the LPFC intracortical activity, possibly to assist in the control of intelligent wheelchairs. In addition, knowing the region of interest within a tailored map, could control a robotic apparatus, assistive device, or even provide clues on what the user intends to do depending on the content of the selected location.

In our study, the virtual environment did not include landmarks other than the end goal colored disk. This disk became visible once the end of the maze corridor was reached and was located in one of two possible branches depending on the trial context. In such task scenario, we suspect the animal used an egocentric reference frame where the coded spatial positions in the maze were relative to the estimated end goal or the maze intersection points. Future research should add landmarks through the maze and investigate the effect on the spatial locations decoding accuracy in an allocentric reference frame.

4.2. Maximizing performance for iBCI systems

In real-time and critical application such as an iBCI, the decoder accuracy must be reliable since the failures will significantly impact the user's satisfaction and its benefit. In navigation, reaching a future position depends on the current location, and the associated probability between them. Such processes which retain no memory of past states are called Markov processes (Norris 1998). Markov chains, which are finite sets of state transition probabilities, have been used to model cellular signal processing (Said *et al* 2003), to forecast daily precipitation (Bojar *et al* 2018), and to simulate sleep electroencephalography patterns (Zung *et al* 1965). We evaluated the possibility to improve the decoding performance by modifying the locations' probabilities predicted by the SVM with the transition probabilities embedded in the Markov chain. As expected, with a designed Markov chain favoring the forward navigation, we obtained valuable prediction accuracy improvements. Future work should look at how the state transition probability matrix of the Markov chain could be dynamically updated based on past trials, to better represent the environment and navigational constraints.

4.3. Canonical discriminant analysis

To reduce processing requirement, we further investigated how a canonical discriminant analysis could optimize the contributions of multi-unit activity for locations' selectivity while reducing the overall size of the feature set. The result for individual blocks and arrays as well as combined blocks and arrays was that the original multi-unit feature set performed better than its projections in canonical space. However, for individual blocks on combined arrays, the projected multi-unit signal performed better overall. The feature set size was reduced by over 11-fold using the canonical space which may be important in the design of an iBCI system.

4.4. BCI application

In principle, we reasoned that as reported by Downey *et al* (2016), combining information from both, a BCI system and vision-guided autonomous robotics, can improve the control of an assistive device used for navigation or other purposes. One may ask, could LPFC activity contribute to a BCI? The LPFC has been classically associated with high level cognition, planning and executive function (Miller and Cohen 2001, Fuster 2015). Neuronal ensembles in the LPFC, the area we recorded from in this study, encode spatial attention (Tremblay *et al* 2015, Backen *et al* 2018), movement goals (Boulay *et al* 2015), and short-term memory (Leavitt *et al* 2017b) in spatiocentric coordinates, rather than in retinal coordinates, as many areas located more posteriorly in the brain (Crawford *et al* 2003). Moreover, LPFC ensemble codes reflect the biases in space processing observed during behavior (Leavitt *et al* 2017a). Finally, LPFC activity undergoes gain control within the area microcircuit, which calibrates neural activity for changes in environmental variables such as stimulus intensity (Bullock *et al* 2017, Duong *et al* 2019). Together with its location at the top of the sensory processing hierarchy (Felleman and Essen 1991), the findings reported in LPFC electrophysiological studies in non-human primates indicate that the computations performed in this area are at the final stage of visual and perceptual integration in primate brains such as the ones of macaques and humans. If a BCI were to incorporate aspects of cognition and executive control, a combination of LPFC and motor cortex

interfaces may achieve more functionality than either of them alone (Andersen *et al* 2004, Pesaran *et al* 2006, Andersen *et al* 2010).

One specific example of how LPFC activity can aid a motor cortex BCI is to encode desired locations in space-centered coordinates while navigating through an environment (in our scenario the virtual maze), and planning multiple sequential actions (e.g. visiting different locations in a sequence). For a BCI to assist in such tasks in the presence of eye movements and possibly changes in body position, it would be ideal to encode goals in space-centered frames, and it must be robust enough to ignore the interference produced by eye movements. LPFC ensembles encode goals in a space-centered frame independently of eye and arm movements (Roussy *et al* 2022). This intended target location could provide valuable information and possibly improve the control of a navigation system (e.g. a wheelchair) that does sequential actions (Andersen *et al* 2019). Other possible candidates for contributing to cognitive BCIs that encode space-center goals is the posterior parietal cortex (Andersen *et al* 1985). This area has been the target of BCI studies (Andersen *et al* 2004, 2019). Whether BCIs using a combination of posterior parietal cortex, LPFC and motor cortex activity could be more effective for real world tasks than BCIs using one or two of these areas as targets remains speculative. Additional studies must be conducted to address these questions.

5. Conclusion

We examined the spiking and LFP activity recorded from the LPFC of non-human primates while they navigated through a virtual maze. We found that the spatial locations within the maze could be decoded using SVM on those features, particularly well at locations associated with events relevant to the successful completion of the task. We investigated the effects of adding a Markov chain to the SVM decoder and concluded that it significantly improves the location decoding accuracy. Assuming similar activity can be extracted from humans and macaques LPFC during navigation, our results suggest that a goal-based iBCI implant in LPFC could provide useful spatial information to support a navigation-based application for patients with disabilities.

Data availability statement

The data that support the findings of this study are available upon reasonable request from the authors.

Acknowledgments

We are thankful for the support of the neuroscience program at the Ottawa Hospital Research Institute as well as the support from the University of Ottawa Brain and Mind Research Institutes. This work was supported by the Canadian Institute of Health Research Project Grant and Natural Sciences and Engineering Research Council of Canada (NSERC).

Declarations of interest

None.

Ethical statement

The experiment took place and was approved by the Western University and followed all guidelines from the Canadian Council on Animal Care. Physical and psychological assessments of the animals were performed regularly by the research team as well as by veterinary technicians and veterinarians.

ORCID iDs

Renée Johnston https://orcid.org/0000-0002-3402-548X
Mohamad Abbass https://orcid.org/0000-0003-1899-2696
Benjamin Corrigan https://orcid.org/0000-0003-2630-7919
Roberto Gulli https://orcid.org/0000-0001-5983-0672
Julio Martinez-Trujillo https://orcid.org/0000-0003-3338-578X
Adam Sachs https://orcid.org/0000-0002-3630-4562

References

Ajiboye A B *et al* 2017 Restoration of reaching and grasping movements through brain-controlled muscle stimulation in a person with tetraplegia: a proof-of-concept demonstration *Lancet* **389** 1821–30
Al-qaysi Z T, Zaidan B, Zaidan A and Suzani M 2018 A review of disability EEG based wheelchair control system: coherent taxonomy, open challenges and recommendations *Comput. Methods Programs Biomed.* **164** 221–37
Andersen R A, Aflalo T and Kellis S 2019 From thought to action: the brain-machine interface in posterior parietal cortex *Proc. Natl Acad. Sci. USA* **116** 26274–9
Andersen R A, Burdick J W, Musallam S, Pesaran B and Cham J G 2004 Cognitive neural prosthetics *Trends Cogn. Sci.* **8** 486–93
Andersen R A, Essick G K and Siegel R M 1985 Encoding of spatial location by posterior parietal neurons *Science* **230** 456–8
Andersen R A, Hwang E J and Mulliken G H 2010 Cognitive neural prosthetics *Annu. Rev. Psychol.* **61** 169–90
Backen T, Treue S and Martinez-Trujillo J 2018 Encoding of spatial attention by primate prefrontal cortex neuronal ensembles *eNeuro* **5** ENEURO.0372-16.2017
Baraduc P, Duhamel J R and Wirth S 2019 Schema cells in the macaque hippocampus *Science* **363** 635–9
Bojar W, Knopik L, Żarski J, Kuśmierek-Tomaszewska R and Żarski W 2018 Markov chain as a tool for forecasting daily precipitation in the vicinity of the city of Bydgoszcz, Poland *ITM Web Conf.* vol 23 p 3
Boulay C, Pieper F, Leavitt M, Martinez-Trujillo J and Sachs A J 2015 Single-trial decoding of intended eye movement goals from lateral prefrontal cortex neural ensembles *J. Neurophysiol.* **115** 486–99

Bullock K R, Pieper F, Sachs A J and Martinez-Trujillo J C 2017 Visual and presaccadic activity in area 8Ar of the macaque monkey lateral prefrontal cortex *J. Neurophysiol.* **118** 15–28

Buschman T J, Denovellis E L, Diogo C, Bullock D and Miller E K 2012 Synchronous oscillatory neural ensembles for rules in the prefrontal cortex *Neuron* **76** 838–46

Buzsáki G and Moser E I 2013 Memory, navigation and theta rhythm in the hippocampal-entorhinal system *Nat. Neurosci.* **16** 130–8

Chambers J M 1992 Linear models *Statistical Models* ed J M Chambers and T J Hastie (Boca Raton, FL: Chapman & Hall/CRC)

Chen S, Shu X, Wang H, Ding L, Fu J and Jia J 2021 The differences between motor attempt and motor imagery in brain-computer interface accuracy and event-related desynchronization of patients with hemiplegia *Front. Neurorobot.* **15** 1–13

Collinger J L, Wodlinger B, Downey J E, Wang W, Tyler-Kabara E C, Weber D J, McMorland A J, Velliste M, Boninger M L and Schwartz A B 2013 High-performance neuroprosthetic control by an individual with tetraplegia *Lancet* **381** 557–64

Corrigan B W, Gulli R A, Doucet G, Roussy M, Luna R, Sachs A J and Martinez-Trujillo J 2021 Different neural codes serve long and short-term memory functions in primate hippocampus and lateral prefrontal cortex during virtual navigation *bioRxiv Preprint* (https://doi.org/10.1101/2021.08.20.457136) (posted online 21 August 2021)

Crawford J D, Martinez-Trujillo J C and Klier E M 2003 Neural control of three-dimensional eye and head movements *Curr. Opin. Neurobiol.* **13** 655–62

Curtis C E and D'Esposito M 2003 Persistent activity in the prefrontal cortex during working memory *Trends Cogn. Sci.* **7** 415–23

Doucet G, Gulli R A and Martinez-Trujillo J 2016 Cross-species 3D virtual reality toolbox for visual and cognitive experiments *J. Neurosci. Methods* **266** 84–93

Downey J E, Weiss J M, Muelling K, Venkatraman A, Valois J S, Hebert M, Bagnell J A, Schwartz A B and Collinger J L and 2016 Blending of brain-machine interface and vision-guided autonomous robotics improves neuroprosthetic arm performance during grasping *J. NeuroEng. Rehabil.* **13** 1–12

Duong L, Leavitt M, Pieper F, Sachs A and Martinez-Trujillo J 2019 A normalization circuit underlying coding of spatial attention in primate lateral prefrontal cortex *Eneuro* **6** ENEURO.0301-18.2019

Ekstrom A D, Kahana M J, Caplan J B, Fields T A, Isham E A, Newman E L and Fried I 2003 Cellular networks underlying human spatial navigation *Nature* **425** 184–7

Fan J M, Nuyujukian P, Kao J C, Chestek C A, Ryu S I and Shenoy K 2014 Intention estimation in brain-machine interfaces *J. Neural Eng.* **11** 016004

Fan R E, Chang K W, Hsieh C J, Wang X R and Lin C J 2008 LIBLINEAR: a library for large linear classification *J. Mach. Learn. Res.* **9** 1871–4

Felleman D J and Essen D C V 1991 Distributed hierarchical processing in the primate cerebral cortex *Cereb. Cortex* **1** 1–47

Flint R D, Lindberg E W, Jordan L R, Miller L E and Slutzky M W 2012 Accurate decoding of reaching movements from field potentials in the absence of spikes *J. Neural Eng.* **9** 1–22

Friendly M and Fox J 2020 Candisc: visualizing generalized canonical discriminant and canonical correlation analysis, R package version 0.8–3

Fuster J M 2015 Anatomy of the prefrontal cortex *The Prefrontal Cortex* (Amsterdam: Elsevier) pp 9–62

Gulli R A, Duong L R, Corrigan B W, Doucet G, Williams S, Fusi S and Martinez-Trujillo J 2020 Context-dependent representations of objects and space in the primate hippocampus during virtual navigation *Nat. Neurosci.* **23** 103–12

Jansen-Osmann P 2002 Using desktop virtual environments to investigate the role of landmarks *Comput. Hum. Behav.* **18** 427–36

Johnston R, Doucet G, Boulay C, Miller K, Martinez-Trujillo J and Sachs A 2021 Decoding saccade intention from primate prefrontal cortical local field potentials using spectral, spatial, and temporal dimensionality reduction *Int. J. Neural Syst.* **31** 1–19

Jung M W, Qin Y, McNaughton B L and Barnes C A 1998 Firing characteristics of deep layer neurons in prefrontal cortex in rats performing spatial working memory tasks *Cereb. Cortex* **8** 437–50

Kang X, Sarma S V, Santaniello S, Schieber M and Thakor N V 2015 Task-independent cognitive state transition detection from cortical neurons during 3D reach-to-grasp movements *IEEE Trans. Neural Syst. Rehabil. Eng.* **23** 676–82

Kao J C, Nuyujukian P, Ryu S I and Shenoy K 2017 A high-performance neural prosthesis incorporating discrete state selection with hidden Markov models *IEEE Trans. Biomed. Eng.* **64** 935–45

Leavitt M L, Pieper F, Sachs A J and Martinez-Trujillo J 2017a A quadrantic bias in prefrontal representation of visual-mnemonic space *Cereb. Cortex* **52** 1–17

Leavitt M L, Pieper F, Sachs A J and Martinez-Trujillo J 2017b Correlated variability modifies working memory fidelity in primate prefrontal neuronal ensembles *Proc. Natl Acad. Sci. USA* **114** E2494–503

Lee S A 2017 The boundary-based view of spatial cognition: a synthesis *Curr. Opin. Behav. Sci.* **16** 58–65

Lennert T and Martinez-Trujillo J 2013 Prefrontal neurons of opposite spatial preference display distinct target selection dynamics *J. Neurosci.* **33** 9520–9

Leon M I and Shadlen M N 1999 Effect of expected reward magnitude on the response of neurons in the dorsolateral prefrontal cortex of the macaque *Neuron* **24** 415–25

Markowitz D A, Wong Y T, Gray C M and Pesaran B 2011 Optimizing the decoding of movement goals from local field potentials in macaque cortex *J. Neurosci.* **31** 18412–22

May M and Klatzky R L 2000 Path integration while ignoring irrelevant movement *J. Exp. Psychol.: Learn. Mem. Cogn.* **26** 169–86

Maynard E M, Nordhausen C T and Normann R A 1997 The Utah intracortical electrode array: a recording structure for potential brain-computer interfaces *Electroencephalogr. Clin. Neurophysiol.* **102** 228–39

Mendoza-Halliday D and Martinez-Trujillo J 2017 Neuronal population coding of perceived and memorized visual features in the lateral prefrontal cortex *Nat. Commun.* **8** 1–13

Miller E K and Cohen J D 2001 An integrative theory of prefrontal cortex function *Annu. Rev. Neurosci.* **24** 167–202

Miller E K, Lundqvist M and Bastos A M 2018 Working memory 2.0 *Neuron* **100** 463–75

Miller K J, Honey C J, Hermes D, Rao R P N, denNijs M and Ojemann J G 2014 Broadband changes in the cortical surface potential track activation of functionally diverse neuronal populations *Neuroimage* **85** 711–20

Miller K J, Zanos S, Fetz E E, Den Nijs M and Ojemann J G 2009 Decoupling the cortical power spectrum reveals real-time representation of individual finger movements in humans *J. Neurosci.* **29** 3132–7

Nakayama Y, Yamagata T, Tanji J and Hoshi E 2008 Transformation of a virtual action plan into a motor plan in the premotor cortex *J. Neurosci.* **28** 10287–97

Normann R A, Maynard E M, Rousche P J and Warren D J 1999 A neural interface for a cortical vision prosthesis *Vis. Res.* **39** 2577–87

Norris J R 1998 *Markov Chains (No. 2)* (Cambridge: Cambridge University Press)

O'Keefe J and Dostrovsky J 1971 Short communications the hippocampus as a spatial map. Preliminary evidence from unit activity in the freely-moving rat *Brain Res.* **34** 171–5

Pandarinath C, Nuyujukian P, Blabe C H, Sorice B L, Saab J, Willett F R, Hochberg L, Shenoy K and Henderson J M 2017

High performance communication by people with paralysis using an intracortical brain-computer interface *Elife* **6** 805–15

Pesaran B, Musallam S and Andersen R A 2006 Cognitive neural prosthetics *Curr. Biol.* **16** 77–80

Petrides M 2005 Lateral prefrontal cortex: architectonic and functional organization *Phil. Trans. R. Soc.* B **360** 781–95

Rajangam S, Tseng P H, Yin A, Lehew G, Schwarz D, Lebedev M A and Nicolelis A Y 2016 Wireless cortical brain-machine interface for whole-body navigation in primates *Sci. Rep.* **6** 1–13

Ramsay J O and Silverman W 1997 Canonical correlation and discriminant analysis, in functional data analysis *Springer Series in Statistics* (New York: Springer)

Rolls E T and Wirth S 2018 Spatial representations in the primate hippocampus, and their functions in memory and navigation *Prog. Neurobiol.* **171** 90–113

Rolls E T and Xiang J Z 2006 Spatial view cells in the primate hippocampus, and memory recall *Rev. Neurosci.* **17** 175–200

Roussy M, Corrigan B, Luna R, Gulli R A, Sachs A J, Palaniyappan L and Martinez-Trujillo J C 2022 Stable working memory and perceptual representations in macaque lateral prefrontal cortex during naturalistic vision *J. Neurosci.* **42** JN-RM-0597-22

Roussy M, Luna R, Duong L, Corrigan B, Gulli R A, Nogueira R, Moreno-Bote R, Sachs A J, Palaniyappan L and Martinez-Trujillo J C 2021 Ketamine disrupts naturalistic coding of working memory in primate lateral prefrontal cortex networks *Mol. Psychiatry* **26** 6688–703

Said M R, Oppenheim A V and Lauffenburger D A 2003 Modeling cellular signal processing using interacting Markov chains *ICASSP, IEEE Int. Conf. Acoust. Speech Signal Process.—Proc.* vol 6 pp 41–44

Santhanam G, Ryu S I, Yu B M, Afshar A and Shenoy K 2006 A high-performance brain-computer interface *Nature* **442** 195–8

Shenoy K, Sahani M and Churchland M M 2013 Cortical control of arm movements: a dynamical systems perspective *Annu. Rev. Neurosci.* **36** 337–59

Spellman T, Rigotti M, Ahmari S E, Fusi S, Gogos J A and Gordon J A 2015 Hippocampal-prefrontal input supports spatial encoding in working memory *Nature* **522** 309–14

Sumsky S L, Schieber M H, Thakor N V, Sarma S V and Santaniello S 2017 Decoding kinematics using task-independent movement-phase-specific encoding models *IEEE Trans. Neural Syst. Rehabil. Eng.* **25** 2122–32

Tremblay S, Pieper F, Sachs A and Martinez-Trujillo J 2015 Attentional filtering of visual information by neuronal ensembles in the primate lateral prefrontal cortex *Neuron* **85** 202–15

Vogel P, Hahn J, Duvarci S and Sigurdsson T 2022 Prefrontal pyramidal neurons are critical for all phases of working memory *Cell Rep.* **39** 110659

Wallis J D, Anderson K C and Miller E K 2001 Single neurons in prefrontal cortex encode abstract roles *Nature* **411** 953–6

Watanabe M 2007 Role of anticipated reward in cognitive behavioral control *Curr. Opin. Neurobiol.* **17** 213–9

Wilcoxon F 1945 Individual comparisons by ranking methods *Biometr. Bull.* **1** 196–202

Wilkinson N and Rogers C E 1973 Symbolic description of factorial models for analysis of variance *J. Appl. Stat.* **22** 392–9

Zung W, Naylor T, Gianturco D and Wilson W 1965 Computer simulation of sleep EEG patterns with a Markov chain model *Recent Adv. Biol. Psychiatry* **8** 335–55